JACS
JOURNAL OF THE AMERICAN CHEMICAL SOCIETY

Communication

pubs.acs.org/JACS

Digital, Ultrasensitive, End-Point Protein Measurements with Large Dynamic Range via Brownian Trapping with Drift

Shencheng Ge,† Weishan Liu,† Travis Schlappi, and Rustem F. Ismagilov*

Division of Chemistry and Chemical Engineering, California Institute of Technology, 1200 East California Boulevard, Pasadena, California 91125, United States

Supporting Information

ABSTRACT: This communication shows that the concept of Brownian trapping with drift can be applied to improve quantitative molecular measurements. It has the potential to combine the robustness of end-point spatially resolved readouts, the ultrasensitivity of digital single-molecule measurements, and the large dynamic range of qPCR; furthermore, at low concentrations of analytes, it can provide a direct comparison of the signals arising from the analyte and from the background. It relies on the finding that molecules simultaneously diffusing, drifting (via slow flow), and binding to an array of nonsaturable surface traps have an exponentially decreasing probability of escaping the traps over time and therefore give rise to an exponentially decaying distribution of trapped molecules in space. This concept was tested with enzyme and protein measurements in a microfluidic device.

Digital single-molecule measurements,[1] such as digital PCR (dPCR)[2] and digital immunoassays,[3] compartmentalize molecules of the target analyte and perform a detection reaction providing an "on" or "off" signal for each compartment (digital unit). Analyte concentration is then quantified by counting the signals and using a Poisson distribution. This methodology has been used in a wide range of applications to detect nucleic acids and proteins with ultrasensitivity.[4]

One limitation of digital measurements is that the dynamic range (i.e., the range between the lowest and highest concentrations in a sample that can be measured) is limited by the number of digital units in the assay. Quantitative real-time PCR (qPCR) has a much wider dynamic range because input concentration is calculated as an exponential function of the qPCR output; however, this method is less convenient than an end-point measurement. Dynamic range in dPCR can be increased by introducing very large numbers of digital units (compartments)[5] or using digital units of multiple sizes,[6] which increases the dynamic range by more than ~100-fold. However, the multivolume strategy is not as effective for digital immunoassays that lack the exponential amplification of PCR. One strategy to improve dynamic range for digital immunoassays involves combining the digital readout with the analog readout, which has increased the dynamic range from 2.5 logs to 4.1 logs.[7] Such improvement is desired, for example, in assays for the biomarker glial fibrillary acidic protein (GFAP) in traumatic brain injury.[8]

Our goal was to test whether it would be possible to combine into a single measurement (i) the high sensitivity of digital assays, in which individual molecules give rise to on/off signals, (ii) the broad dynamic range (~10^8) characteristic of a technique like qPCR, in which large changes in the input concentration give rise to logarithmically smaller changes in the output (Cq); in other words, input concentration is calculated as an exponential function of the output; and (iii) a readout in which the input number of molecules is quantified by an end-point spatial signal, which is more robust than the temporal signal from kinetic real time assays.[9]

Here, we tested whether our goal could be reached by implementing the concept of Brownian trapping with drift[10] in a microfluidic device (Figure 1). In Brownian trapping, target

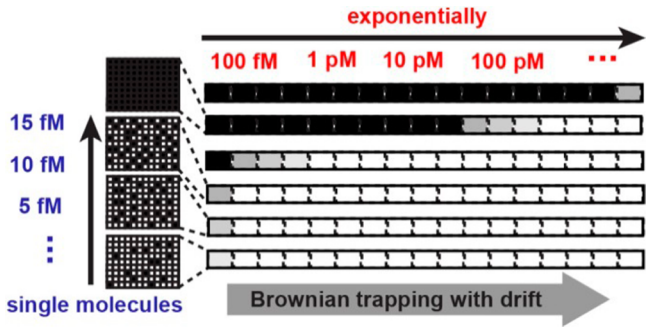

Figure 1. Conceptual schematic of a digital measurement using Brownian trapping with drift. This concept aims to combine the ultrasensitivity of digital detection (shown in blue) with the broad dynamic range inherent in real-time PCR assays, in which large changes in the input concentration give rise to logarithmically smaller changes in the output (shown in red).

objects move by diffusion and are captured by traps of radius ρ and trap density ν. When Brownian trapping is combined with directional drift U of the target objects,[10] the probability of a target object eluding the traps, $P(t;U,\nu,\rho)$, decays exponentially at long times with decay rate $\lambda(U,\nu,\rho)$, a function of U,ν and ρ (eq 1).[10c]

$$P(t;\ U,\ \nu,\ \rho) \approx \exp(-\lambda(U,\ \nu,\ \rho)t) \qquad (1)$$

This exponential decay only occurs when traps are not saturated by the targets during the experiment. This phenomenon has been analyzed mathematically in the context of charge

Received: July 31, 2014
Published: October 7, 2014

   dx.doi.org/10.1021/ja507849b | J. Am. Chem. Soc. 2014, 136, 14662−14665

carriers in semiconductors,[10a] diffusion-controlled reactions in the presence of a biasing field,[10d] and photoluminescence in the presence of electrical bias,[10b] but has not been applied to molecular analyses.

To test Brownian trapping in a digital immunoassay (Figure 1), we envisioned the target object was a protein analyte molecule, and the traps were areas containing a capture reagent, such as an antibody. Traps were distributed on the channel surface, configured to act as digital units and grouped into regions (Figure 2). We envisioned introducing drift using a gentle

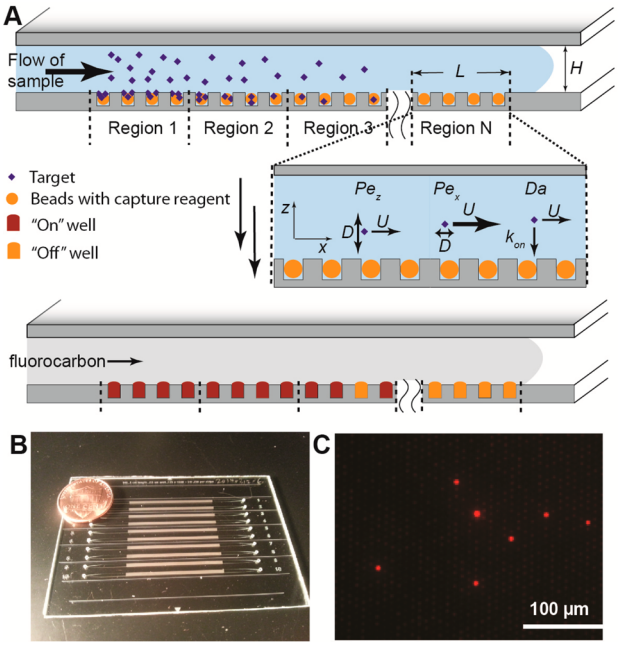

Figure 2. Experimental design to test the concept of digital measurements based on Brownian trapping with advective drift. (A) Schematic of the design, which features a shallow channel (50 μm) on top of an array of microwells. A bead (orange) coated with a capture reagent (e.g., an antibody), is placed in each microwell. The channel guides the flow of the sample over the microwells, and target molecules (blue) are captured by the beads. After labeling, the microwells are compartmentalized by fluorocarbon for digital readout. (B) A photograph of an assembled device with 10 parallel arrays. (C) A fluorescent image of the digital readout.

advective flow of solution through the microfluidic channel. Under these conditions, each trap provides a digital on/off readout (Figure 2). At low concentrations, we hypothesized that most analyte molecules would be trapped at the beginning of the channel and concentration could be estimated using the conventional Poisson statistics of digital immunoassays.[3c] However, at high concentrations, we hypothesized that analyte concentration could be estimated using a spatial analogue of eq 1 (see Supporting Information S1).

Our experimental design (Figure 2) satisfied four criteria arising from the concept of Brownian trapping with drift[10] (we have not optimized experimental parameters, instead choosing one experimentally convenient combination; see Supporting Information). (i) Drift should dominate over diffusion of the protein target (diffusion coefficient $D \approx 10^{-11}$ m^2/s) along the flow direction x (here, Péclet number $Pe_x = UL/D \approx 10^3$), with each region sufficiently long ($L \approx 10^{-3}$ m) and flow sufficiently high ($U \approx 10^{-5}$ m/s). Under these conditions, the exponential decay over time (eq 1) would be manifested as an exponential decay over space (Figure 1), effectively converting temporal distribution into spatial distribution. (ii) At the same time, flow should be slow enough that diffusion of the protein from the top to the bottom of the channel (H) is not slower than flow over one region ($Pe_z = (U/L)/(D/H^2) \approx 2.5$); (iii) each trap should have high binding capacity so it is not saturated by the targets during the experiment. Beads used for digital immunoassays[3,4a,c,d] satisfy this criterion. This criterion has not been met previously in innovative quantification approaches that flow a sample through a microfluidic channel to generate a density gradient on the channel surface.[11] In such experiments, the protein signal decayed linearly over channel length instead of exponentially. (iv) The Damköhler number $Da \approx k_{on}[\mathrm{Ab}]L/U$, (estimated to be ~1, [Ab] is the concentration of the capture reagent) should be close to or greater than 1 to enable rapid capture of the target molecules once they diffuse to the traps.

We tested this concept experimentally using a glass SlipChip device[12] (Figure 2B), which contained 10 parallel arrays created by dry-etching with C_4F_8, each containing 540,000 microwells grouped into regions. Each well was loaded with a single bead coated with a capture antibody. We took advantage of the relative movement of the two plates of the SlipChip to achieve uniform and near-complete bead loading. As the sample passed over the wells, the protein targets were trapped on the beads, rapidly depleting the target analyte from the flowing solution.

We first used a simple model system with biotin-modified β-galactosidase as the target analyte (3 μL samples in a range of concentrations) and streptavidin-coated beads as the capture agents. First, the enzyme solution was flown over the beads through the channel at a velocity of 17 μm/s for 1 h. Then a solution of fluorogenic substrate resorufin β-D-galactopyranoside (RGP) was injected into the channel, immediately followed by a flow of FC40 to compartmentalize the beads in the microwells. Analyte concentration was estimated using the fraction of beads that captured at least one molecule (positive fraction of beads)[3,4a,c,d] (Figure 3A). Analyte molecules were preferentially captured in the upstream regions, so low analyte concentrations were quantified by the positive fraction of wells located in the first capture region (Figure 3B). We calculated the limit of detection (LOD) from three times the standard deviation of the experimentally measured background signal to be 9 aM. At higher concentrations, as is established,[7] we used a fraction of 0.8 as the practical upper limit, corresponding to 20 fM (Figure 3B).

At high analyte concentrations, beads in the upstream regions contained many analyte molecules, precluding end-point digital quantification using those regions (we emphasize that beads, which could bind ~10^5 analyte molecules, were not expected to be fully saturated with analyte under those conditions). Analyte molecules were also captured in the downstream regions. As predicted, we observed that exponentially increasing analyte concentration gave rise to an approximately linear shift in the region where the capture curve crossed a threshold value of positive fraction (Figure 3A,C,D). We refer to this region as Rq (region of quantification), analogous to Cq used in qPCR; its position depends on the value of the chosen threshold. Using a low threshold of 0.07 positive fraction (Figure 3C) provided a dynamic range that overlapped well with the digital calibration curve (Figure 3B) while extending it by ~10^2 (above 1 pM). Using a high threshold of 0.8 positive fraction (Figure 3D) further extended the dynamic range above 0.3 nM. The combined dynamic range was ~4 × 10^7-fold, with a sensitivity of ~20 molecules in 3 μL.

dx.doi.org/10.1021/ja507849b | J. Am. Chem. Soc. 2014, 136, 14662−14665

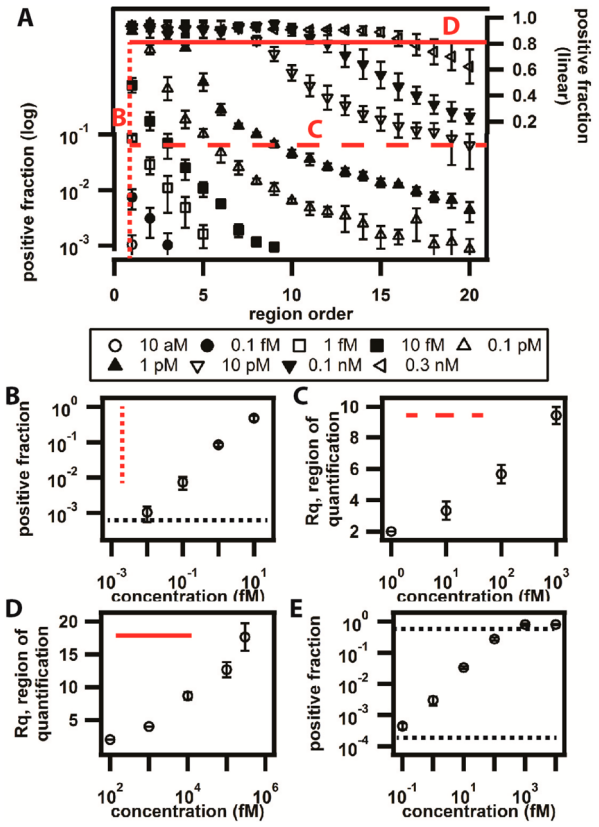

Figure 3. Experimental evaluation of the digital protein measurement with Brownian trapping with drift. (A) Capture curves of biotinylated β-galactosidase with concentrations ranging from 10 aM to 0.3 nM. The red lines indicate data replotted in panels B, C, and D. (B) A plot of the positive fraction of beads at the first region vs low analyte concentrations, from 9 aM to 20 fM. The dotted horizontal line represents the lower limit of quantification. (C) A plot of Rq (region of quantification, threshold of 0.07 positive fraction) vs the logarithm of analyte concentration ranging from 1 fM to 1 pM. (D) A plot of Rq (threshold of 0.8 positive fraction) vs the logarithm of analyte concentration ranging from 0.1 pM to 0.3 nM. (E) A plot of the positive fraction of beads in the entire array in a standard digital protein assay at concentrations ranging from 0.1 fM to 10 nM. The dotted horizontal lines represent the upper and lower limits of quantification.

For comparison, in an identical SlipChip device we performed a standard digital protein assay in which the whole solution was injected into the device rapidly and kept stationary during a 1 h incubation, followed by detection as described above. The calculated dynamic range in this stationary assay ranged from 0.02 fM to 0.5 pM, demonstrating a range of ~20,000-fold, and a sensitivity of ~30 molecules (Figure 3E). Therefore, the digital measurement based on Brownian trapping with drift showed similar sensitivity but a more than 1000-fold improvement in dynamic range relative to the stationary digital assay in the same device.

We then tested how this approach performs in a more complex, clinically relevant immunoassay for a human protein target, TNF-α in a 25% serum. To streamline the multistep ELISA protocol, we adopted a cartridge-with-spacers approach in which all reagents were loaded into a cartridge as plugs separated by FC40 fluorocarbon and air, then delivered into the channel[13] (Figure S3, Supporting Information). We performed calibrations with 8 μL samples containing known TNF-α concentrations in buffered 25% bovine serum. The captured TNF-α molecules were then incubated with 6.5 nM biotinylated detection antibody for 1 h, followed by a 0.5 h incubation with 400 pM streptravidin−galactosidase conjugate and compartmentalization with fluorocarbon.

The measurement preserved ultrasensitivity, with an LOD of 6 fM (Figure 4B). We used this measurement to determine the

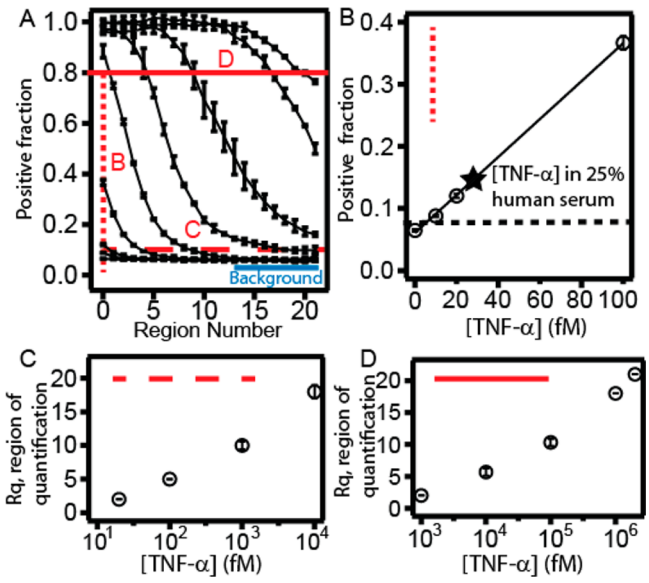

Figure 4. Test of digital measurements based on Brownian trapping with advective drift using human TNF-α. (A) Capture curves obtained from 25% bovine serum samples spiked with increasing concentrations of recombinant TNF-α. From bottom to top, curves represent TNF-α concentrations of 0, 0.01, 0.02, 0.1, 1, 10, 100, 1000, and 2000 pM. The blue line underlines the background signal level directly measured in the assays at low concentrations. (B) A plot of positive bead fraction at low concentration of TNF-α corresponding to the vertical dotted red line in A. The dotted horizontal line represents the background signal + 3SD. The endogenous [TNF-α] in 25% pooled human serum is shown by the star symbol. (C) A plot of Rq (region of quantification, threshold of 0.11 positive fraction) vs the logarithm of TNF-α concentration ranging from 20 fM to 10 pM. (D) A plot of Rq (threshold of 0.8 positive fraction) vs the logarithm of TNF-α concentration ranging from 1 pM to 2 nM.

endogenous concentration of TNF-α in pooled human serum, which is below the detection limit of a conventional ELISA.[14] The measured concentration was 0.031 ± 0.001 pM in 25% serum (Figure 4B), which translates to 0.125 ± 0.004 pM in pure serum. This value is consistent with those determined previously using other single-molecule approaches.[4a,15] At higher concentrations, using a low threshold of 0.11 positive fraction (Figure 4C) provided a dynamic range of ~10^3, and using a high threshold of 0.8 positive fraction (Figure 4D) extended it to 2 nM, for a total dynamic range of ~300,000-fold. While this is wider than the dynamic range achieved previously by digital readout alone (~316-fold)[3c] or the digital and analog readouts combined (~13,000-fold),[7] it is smaller than the dynamic range obtained under the more ideal conditions with enzymes (Figure 3).

We conclude that the concept of Brownian trapping with drift can be used for digital measurements of proteins that combine high sensitivity of digital assays with large dynamic range of qPCR but with an end-point readout. This combination of features has not been demonstrated previously and may be advantageous even for nucleic acid quantification. These findings justify performing future work to understand how combinations

dx.doi.org/10.1021/ja507849b | J. Am. Chem. Soc. 2014, 136, 14662−14665

of values (and their variability) of Pe_x, Pe_z, Da, capture efficiency, flow control,[16] device design, and assay chemistry impact assay performance and enable the design of optimal assays for a given analyte. For example, given the similarity to qPCR, we anticipate lower resolution at higher concentrations where errors in determining the Rq parameter would lead to exponentially larger errors in quantification. It remains to be tested whether methods analogous to those used in qPCR (e.g., the use of spatial or color multiplexing to introduce quantification controls and/or introduce parallel assays targeting multiple epitopes of the same target) could be used with this approach. The low sample consumption and the use of smaller numbers of wells per measurement with a given dynamic range (see Supporting Information S8) would make this approach compatible with spatial multiplexing and single-cell analysis.[17] Finally, we emphasize that at low concentrations of analyte the downstream regions provide a direct measurement of the background signal of the assay (Figure 4A). This feature should be useful to improve assay fidelity.

■ ASSOCIATED CONTENT

Supporting Information

Model evaluation, materials, detailed experimental procedures, and supplemental figures. This material is available free of charge via the Internet at http://pubs.acs.org.

■ AUTHOR INFORMATION

Corresponding Author

*E-mail: rustem.admin@caltech.edu.

Author Contributions

†These authors contributed equally to this work.

Notes

The authors declare the following competing financial interest(s): R.F.I. has a financial interest in SlipChip Corp.

■ ACKNOWLEDGMENTS

This work was supported by DARPA Cooperative Agreement HR0011-11-2-0006. We thank Kevin Kan, Melissa Melendes, Shawn Hsu, Songzi Kou, Alexander Tucker-Schwartz, Mikhail Karymov, Jason Kreutz and Stephanie McCalla for discussions and experimental help, and Natasha Shelby for contributions to writing and editing this manuscript.

■ REFERENCES

(1) (a) Li, Z. H.; Hayman, R. B.; Walt, D. R. *J. Am. Chem. Soc.* **2008**, *130*, 12622. (b) Rissin, D. M.; Gorris, H. H.; Walt, D. R. *J. Am. Chem. Soc.* **2008**, *130*, 5349. (c) Rissin, D. M.; Walt, D. R. *J. Am. Chem. Soc.* **2006**, *128*, 6286. (d) Rondelez, Y.; Tresset, G.; Tabata, K. V.; Arata, H.; Fujita, H.; Takeuchi, S.; Noji, H. *Nat. Biotechnol.* **2005**, *23*, 361.

(2) (a) Vogelstein, B.; Kinzler, K. W. *Proc. Natl. Acad. Sci. U.S.A.* **1999**, *96*, 9236. (b) Sykes, P. J.; Neoh, S. H.; Brisco, M. J.; Hughes, E.; Condon, J.; Morley, A. A. *Biotechniques* **1992**, *13*, 444.

(3) (a) Walt, D. R. *Anal. Chem.* **2013**, *85*, 1258. (b) Chang, L.; Rissin, D. M.; Fournier, D. R.; Piech, T.; Patel, P. P.; Wilson, D. H.; Duffy, D. C. *J. Immunol. Methods* **2012**, *378*, 102. (c) Rissin, D. M.; Kan, C. W.; Campbell, T. G.; Howes, S. C.; Fournier, D. R.; Song, L.; Piech, T.; Patel, P. P.; Chang, L.; Rivnak, A. J.; Ferrell, E. P.; Randall, J. D.; Provuncher, G. K.; Walt, D. R.; Duffy, D. C. *Nat. Biotechnol.* **2010**, *28*, 595. (d) Shim, J. U.; Ranasinghe, R. T.; Smith, C. A.; Ibrahim, S. M.; Hollfelder, F.; Huck, W. T. S.; Klenerman, D.; Abell, C. *ACS Nano* **2013**, *7*, 5955. (e) Witters, D.; Knez, K.; Ceyssens, F.; Puers, R.; Lammertyn, J. *Lab Chip* **2013**, *13*, 2047. (f) Kim, S. H.; Iwai, S.; Araki, S.; Sakakihara, S.; Iino, R.; Noji, H. *Lab Chip* **2012**, *12*, 4986.

(4) (a) Song, L. N.; Hanlon, D. W.; Chang, L.; Provuncher, G. K.; Kan, C. W.; Campbell, T. G.; Fournier, D. R.; Ferrell, E. P.; Rivnak, A. J.; Pink, B. A.; Minnehan, K. A.; Patel, P. P.; Wilson, D. H.; Till, M. A.; Faubion, W. A.; Duffy, D. C. *J. Immunol. Methods* **2011**, *372*, 177. (b) Shen, F.; Davydova, E. K.; Du, W. B.; Kreutz, J. E.; Piepenburg, O.; Ismagilov, R. F. *Anal. Chem.* **2011**, *83*, 3533. (c) Chang, L.; Song, L. N.; Fournier, D. R.; Kan, C. W.; Patel, P. P.; Ferrell, E. P.; Pink, B. A.; Minnehan, K. A.; Hanlon, D. W.; Duffy, D. C.; Wilson, D. H. *J. Virol. Methods* **2013**, *188*, 153. (d) Randall, J.; Mortberg, E.; Provuncher, G. K.; Fournier, D. R.; Duffy, D. C.; Rubertsson, S.; Blennow, K.; Zetterberg, H.; Wilson, D. H. *Resuscitation* **2013**, *84*, 351. (e) Shen, F.; Du, W. B.; Kreutz, J. E.; Fok, A.; Ismagilov, R. F. *Lab Chip* **2010**, *10*, 2666.

(5) (a) Heyries, K. A.; Tropini, C.; VanInsberghe, M.; Doolin, C.; Petriv, O. I.; Singhal, A.; Leung, K.; Hughesman, C. B.; Hansen, C. L. *Nat. Methods* **2011**, *8*, 649. (b) Hatch, A. C.; Fisher, J. S.; Tovar, A. R.; Hsieh, A. T.; Lin, R.; Pentoney, S. L.; Yang, D. L.; Lee, A. P. *Lab Chip* **2011**, *11*, 3838.

(6) (a) Shen, F.; Sun, B.; Kreutz, J. E.; Davydova, E. K.; Du, W. B.; Reddy, P. L.; Joseph, L. J.; Ismagilov, R. F. *J. Am. Chem. Soc.* **2011**, *133*, 17705. (b) Kreutz, J. E.; Munson, T.; Huynh, T.; She, F.; Du, W.; Ismagilov, R. F. *Anal. Chem.* **2011**, *83*, 8158.

(7) Rissin, D. M.; Fournier, D. R.; Piech, T.; Kan, C. W.; Campbell, T. G.; Song, L. A.; Chang, L.; Rivnak, A. J.; Patel, P. P.; Provuncher, G. K.; Ferrell, E. P.; Howes, S. C.; Pink, B. A.; Minnehan, K. A.; Wilson, D. H.; Duffy, D. C. *Anal. Chem.* **2011**, *83*, 2279.

(8) Mayer, C. A.; Brunkhorst, R.; Niessner, M.; Pfeilschifter, W.; Steinmetz, H.; Foerch, C. *PLoS One* **2013**, *8* (4), e62101.

(9) Selck, D. A.; Karymov, M. A.; Sun, B.; Ismagilov, R. F. *Anal. Chem.* **2013**, *85*, 11129.

(10) (a) Grassberger, P.; Procaccia, I. *Phys. Rev. A* **1982**, *26*, 3686. (b) Dulea, M.; Aldea, A. *J. Non-Cryst. Solids* **1987**, *90*, 461. (c) Eisele, T.; Lang, R. *Probab. Theory Relat. Fields* **1987**, *74*, 125. (d) Sanchez, A. D. *Phys. A* **2000**, *284*, 1.

(11) (a) Zhong, M.; Lee, C. Y.; Croushore, C. A.; Sweedler, J. V. *Lab Chip* **2012**, *12*, 2037. (b) Alino, V. J.; Sim, P. H.; Choy, W. T.; Fraser, A.; Yang, K. L. *Langmuir* **2012**, *28*, 17571. (c) Xue, C. Y.; Khan, S. A.; Yang, K. L. *Adv. Mater.* **2009**, *21*, 198. (d) Fosser, K. A.; Nuzzo, R. G. *Anal. Chem.* **2003**, *75*, 5775. (e) Wagner, P.; Zaugg, F.; Mitchink, M. U.S. Patent 20110124130A1, 2011.

(12) (a) Du, W. B.; Li, L.; Nichols, K. P.; Ismagilov, R. F. *Lab Chip* **2009**, *9*, 2286. (b) Huynh, T.; Sun, B.; Li, L.; Nichols, K. P.; Koyner, J. L.; Ismagilov, R. F. *J. Am. Chem. Soc.* **2013**, *135*, 14775. (c) Liu, W.; Chen, D.; Du, W.; Nichols, K. P.; Ismagilov, R. F. *Anal. Chem.* **2010**, *82*, 3276. (d) Sakakihara, S.; Araki, S.; Iino, R.; Noji, H. *Lab Chip* **2010**, *10*, 3355.

(13) (a) Zheng, B.; Tice, J. D.; Ismagilov, R. F. *Adv. Mater.* **2004**, *16*, 1365. (b) Linder, V.; Sia, S. K.; Whitesides, G. M. *Anal. Chem.* **2005**, *77*, 64. (c) Zheng, B.; Ismagilov, R. F. *Angew. Chem., Int. Ed.* **2005**, *44*, 2520. (d) Chen, D. L.; Ismagilov, R. F. *Curr. Opin. Chem. Biol.* **2006**, *10*, 226.

(14) Martinez-Borra, J.; Lopez-Larrea, C.; Gonzalez, S.; Fuentes, D.; Dieguez, A.; Deschamps, E. M.; Perez-Pariente, J. M.; Lopez-Vazquez, A.; de Francisco, R.; Rodrigo, L. *Am. J. Gastroenterol* **2002**, *97*, 2350.

(15) Todd, J.; Simpson, P.; Estis, J.; Torres, V.; Wub, A. H. B. *Cytokine* **2013**, *64*, 660.

(16) Begolo, S.; Zhukov, D. V.; Selck, D. A.; Li, L.; Ismagilov, R. F. *Lab Chip* **2014**, DOI: 10.1039/C4LC00910J.

(17) Han, Q.; Bagheri, N.; Bradshaw, E. M.; Hafler, D. A.; Lauffenburger, D. A.; Love, J. C. *Proc. Natl. Acad. Sci. U.S.A.* **2012**, *109*, 1607.